Smart Structures and Systems, *Vol. 27, No. 4 (2021) 705-717*
DOI: https://doi.org/10.12989/sss.2021.27.4.705

Performance-based optimization of LQR for active mass damper using symbiotic organisms search

Pei-Ching Chen*, Bryan J. Sugiarto [a] and Kai-Yi Chien [b]

Department of Civil and Construction Engineering, National Taiwan University of Science and Technology, No. 43, Sec. 4, Keelung Rd., Taipei 10607, Taiwan

(*Received August 7, 2020, Revised November 12, 2020, Accepted December 31, 2020*)

Abstract. The linear-quadratic regulator (LQR) has been applied to structural vibration control for decades; however, selection of the weighting matrices of an LQR mostly depends on trial and error. In this study, a novel metaheuristic optimization method named as symbiotic organisms search (SOS) algorithm is applied to tuning LQR weighting matrices for active mass damper (AMD) control systems. A 10-story shear building with an active mass damper installed at the top is adopted as a benchmark for numerical simulation in order to realize the optimization performance considering three objective functions for mitigation of structural acceleration. Two common optimization methods including genetic algorithm (GA), and particle swarm optimization (PSO) are also applied to this benchmark for comparison purposes. Numerical simulation results indicate that SOS is superior to GA and PSO on searching the minimized solution of the three objective functions. Meanwhile, minimizing the square root of the sum of the squares of peak modal acceleration achieves the best control performance of structural acceleration among the three objective functions. In addition, force saturation is proposed and applied in the optimization process such that the control force level is close to the force capacity of AMD under specified earthquake intensity. Furthermore, the control performance of the optimized LQR is compared with that of the LQR designed by applying three common weighting selection methods when the 10-story building is subjected to various earthquake excitations. Simulation results demonstrate that the optimized LQR significantly outperforms the three LQRs on structural acceleration responses as expected and reduces story drift slightly better than the three LQRs. Finally, the performance-based optimized LQR is experimentally validated by conducting shake table testing in the laboratory. The experimental results and structural control performance are discussed and summarized thoroughly.

Keywords: symbiotic organisms search; linear-quadratic regulator; weighting optimization; active mass damper; structural control; shake table testing

1. Introduction

Structural control systems have been widely implemented to reduce vibration responses of structures subjected to various types of dynamic loads such as earthquakes and wind loadings. Generally, structural control systems can be categorized into three main strategies based on the operational devices, namely passive, active, and semi-active. To date, various forms of control devices for structural vibration suppression have been proposed by numerous researchers and engineers (Saaed *et al*. 2015). Among them, tuned mass damper (TMD) has been commonly applied to high-rise buildings which consists of a secondary mass connected to the top of the structure through springs and dampers. The vibration frequency of a TMD can be tuned by adjusting the equivalent stiffness of springs; therefore, the TMD is able to effectively dissipate the structural response dominated by the first vibration mode. However, the structural characteristics may be changed during service lifetime which could lead to detuning of the TMD. The TMD control performance could become inferior due to the detuning effect. Hereafter, a multiple tuned mass damper (MTMD) has been proposed to reduce the detuning problem which consists of multiple single-degree-of-freedom (SDOF) TMDs arranged in parallel to cope with one structural vibration mode, providing a broad bandwidth to cover the variation of the structural vibration frequency (Xu and Igusa 1992). Optimization of individual stiffness and damping parameters of a MTMD system has been studied using artificial bee colony algorithm (Bozer and Özsarıyıldız 2018). Alternatively, active mass damper (AMD) in which the mass is connected to the structure through a hydraulic actuator has been proposed to improve the applicability for a broad bandwidth through active control mechanism.

Various control algorithms for AMD have been proposed and validated for the past decades. Chang and Yang (1995) computed the control force of AMD by using displacement, velocity and acceleration measurements. Dyke *et al*. (1996) applied H2/LQG frequency domain control method employed acceleration feedback to drive the AMD installed on a 3-story small-scale specimen. Experimental results demonstrated that the controller was able to reduce acceleration responses effectively. Cao *et al*.

*Corresponding author, Associate Professor,
E-mail: peichingchen@mail.ntust.edu.tw
[a] Graduate Student, E-mail: m10605823@mail.ntust.edu.tw
[b] Graduate Student, E-mail: m10705332@mail.ntust.edu.tw

ISSN: 1738-1584 (Print), 1738-1991 (Online)

(1998) used the linear-quadratic regulator (LQR) and a nonlinear feedback control algorithm to drive the AMD installed on a tall tower. Bani-Hani (2007) applied a robust neural network methodology to AMD for vibration mitigation of tall building under wind excitation. Lim (2008) applied a robust saturation controller to AMD to control linear structures which considered saturation of control input and structured parameter uncertainties. Cao and Li (2012) applied H∞ robust control strategy to suppress the structural vibration and enhance the stability of the AMD control system. Chen and Casciati (2012) used wireless sensors for feedback control of the AMD system. Chen and Yang (2014) proposed a multilayer feedforward neural network with the modified Newton method for structural vibration suppression. Jang *et al*. (2014) investigated the feasibility of an AMD using time delay control algorithm and demonstrated that the proposed control scheme effectively reduced the acceleration response of the building structure through numerical simulation. Yang *et al*. (2017) proposed a multi-modal negative acceleration feedback control to suppress multiple modal responses using a single AMD. Li *et al*. (2019) reduced vibration of a nonlinear structure by applying an adaptive control of AMD based on model reference sliding-mode control. The structural vibration due to dynamic loading can be effectively mitigated by applying these control algorithms.

Among the aforementioned control approaches, LQR has been recognized as one of the most effective control algorithms to achieve optimal control performance of structures subjected to earthquakes. In order to obtain the optimal control force imposed on the structure, LQR minimizes a cost function formulated by weighted states and control inputs. However, it is difficult to tune the weightings of LQR algorithm effectively since identifying the correlation between the weightings and the structural response may not be straightforward. Generally, designers use their experience combined with trial and error to determine the weightings which could be ineffective and limited to achieve ideal control performance. Moghaddasie and Jalaeefar (2019) adopted an energy-type weighting matrix with a regulating parameter for LQR design. A trial-and-error procedure was conducted to determine the optimal regulating parameter for each SDOF system with specific structural characteristics and maximum control force. Then, the method was extended to multi-degree-of-freedom (MDOF) structures in modal space. Although the method provided a step-by-step approach to determine the weighting matrices of LQR, it was difficult to implement in real practice. As a result, systematic and automatic tuning of weightings may be essential and helpful to completing the design of LQR. Metaheuristic optimization algorithms are alternatives to tune the weighting matrices of LQR effectively and achieve optimal results with respect to user-defined objective functions.

Metaheuristic optimization is a high-level procedure specially designated for seeking an approximate but excellent enough solution of an optimization problem. To date, numerous metaheuristic optimization algorithms have been developed, proposed, and applied for engineering optimization problems. Nearly all the metaheuristic algorithms are nature-inspired and need no gradient information. Random variables are utilized in the algorithms in order to seek an optimized parameter set with respect to one or multiple objectives through an iterative generation process and learning strategies. Some of them have been applied to the determination of LQR weighting matrices for system control in the past, and the most frequently-adopted algorithms are the genetic algorithm (GA) and particle swarm optimization (PSO). For GA applications, Tan *el al*. (2005) applied GA to optimize both the placement of active devices and weighting matrix of the H2/LQG controller through numerical studies. Simulation results indicated that the placement of active devices was highly dependent on the desired control performance and the capacity of active device. A tradeoff between economy and performance was able to be considered in the proposed methodology. Zaeri *et al*. (2007) improved the performance of a Cûk converter by applying LQR in which the weighting matrices were selected based on GA. The results showed that the GA-based LQR had better overshoot, oscillation, settling time, and steady-state error compared to manually-tuned LQR. Wongsathan and Sirima (2008) applied GA to optimize the weighting matrices of LQR for an inverted pendulum system (IPS), which is a marginally stable and highly nonlinear system for validating control algorithms in control engineering fields. Research results showed that GA-optimized LQR performed better than the experimental LQR in controlling the IPS. Bhushan *et al*. (2016) implemented GA in doubly-fed induction generator systems to optimize the weighting matrices of the LQR. On the other hand, for PSO applications, Xiong and Wan (2010) applied PSO for the simulation of a double IPS to optimize the LQR weighting matrices. The result showed that PSO-based LQR was superior to those LQR with trial and error in terms of position and angle control. Duan and Sun (2013) utilized PSO to optimize LQR weighting matrices for controlling the hover and stare state of a micro air vehicle. Experimental results indicated that PSO-based LQR was able to enhance the surveillance performance of the micro air vehicle efficiently. Amini *et al*. (2013) proposed wavelet PSO-based LQR algorithm for optimal structural control using AMD in which discrete wavelet was used to obtain the local energy distribution of the vibration over the frequency bands and PSO was used to determine the weighting matrices of LQR. In addition to GA and PSO, other metaheuristic optimization algorithms have been adopted for the selection of LQR weighting matrices. Wang et al. (2014) applied artificial bee colony algorithm to optimize LQR weighting matrices for circular-rail double IPS. Jacknoon and Abido (2017) used ant colony optimization for tuning LQR weightings and proportional-integral-derivative (PID) gains in order to control the vertical angle of an IPS. These applications of metaheuristic algorithms for the weighting selection of LQR have successfully demonstrated an approach to optimize the LQR performance in various aspects.

A novel and simple metaheuristic algorithm named as symbiotic organisms search (SOS) proposed by Cheng and Prayogo (2014) has been applied or modified to solve

various engineering problems, in particular, electrical and mechanical control engineering problems. Meanwhile, SOS demonstrates superior optimization performance against other metaheuristic optimization algorithms in these problems. For control application, Çelik and Durgut (2018) attempted to apply SOS to PID controller design through a new cost function in which both time-domain and frequency-domain parameters were considered. Tejani *et al*. (2019) applied a modified SOS algorithm to tune the PID controller of a DC motor speed-controlled system. The control performance was evaluated by simulations and experiments and compared with PSO, GA, and Ziegler-Nichols tuning methods. Results indicated that the SOS algorithm was better than other algorithms in tracking performance and capability of rejecting the load disturbance of the control system.

In this study, SOS is adopted to determine the weighting matrices of LQR for active structural control using AMD. This is the first SOS application and evaluation on designing and validating LQR for active structural control. The states to be regulated by LQR are converted into modal configuration. The study contains three stages. First, a 10-story benchmark building controlled by an AMD is used to investigate the effectiveness of various metaheuristic algorithms on different objective functions. Three objective functions are selected to seek the best one for suppressing structural acceleration. They are the root-mean-square (RMS) of the sum of the selected modal acceleration, the maximum of the sum of the selected modal acceleration, and the square root of sum of squares (SRSS) of maximum acceleration of the selected modes. The weightings of LQR are determined by minimizing the three objective functions using GA, PSO, and SOS. In addition, force saturation is considered in the optimization process in order to achieve a control force level that is close to the actuator force capacity under the design earthquake intensity. Afterwards, the simulation results are compared and discussed thoroughly. The corresponding control performance is then compared with three common LQR weighting matrices selection methods. Finally, validating experiments are performed in the structural laboratory and the results are summarized and concluded.

2. Modal LQR control

Modal control, which describes a structural system in modal coordinates is one of the common control approaches to suppress structural vibration. It is realized that the dynamic response of a building is dominated by the first few modes; therefore, the active control energy can be mainly focused on the dominating modes through modal control. Controllers for modal control can be designed by using various approaches; however, modal LQR is employed in this study.

2.1 Modal configuration

The equations of motion of a n-degrees-of-freedom shear building equipped with an AMD at the top floor can be written as

$$\boldsymbol{M_s}\ddot{\boldsymbol{x}}(t) + \boldsymbol{C_s}\dot{\boldsymbol{x}}(t) + \boldsymbol{K_s}\boldsymbol{x}(t) = -\boldsymbol{M_s}\boldsymbol{l}\ddot{x}_g(t) + \boldsymbol{\Lambda}u(t) \quad (1)$$

where $\mathbf{M_s}$, $\mathbf{C_s}$, and $\mathbf{K_s}$ are n x n matrices with respect to the mass, damping, and stiffness of the building, respectively; $\mathbf{x}(t)$ is a $n \times 1$ vector that represents the relative displacements at each floor; $u(t)$ is the control force; $\boldsymbol{\Lambda}$ is a $n \times 1$ vector that indicates the location on which the control force of AMD is imposed; $\mathbf{l}$ is a $n \times 1$ vector with all elements equal to unity; and $\ddot{x}_g(t)$ is the ground acceleration. If the states are defined as $\mathbf{z}(t) = [\boldsymbol{x}(t)\ \dot{\boldsymbol{x}}(t)]^T$, the state-space formulation of the building structure can be expressed as

$$\begin{aligned} \dot{\boldsymbol{z}}(t) &= \boldsymbol{A}\boldsymbol{z}(t) + \boldsymbol{B}u(t) + \boldsymbol{E}\ddot{x}_g(t) \\ \boldsymbol{y}(t) &= \boldsymbol{C}\boldsymbol{z}(t) + \boldsymbol{D}u(t) \end{aligned} \quad (2)$$

where the system matrix $\mathbf{A}$, the control force distribution matrix $\mathbf{B}$, and the disturbance location matrix $\mathbf{E}$ are

$$\begin{aligned} \boldsymbol{A} &= \begin{bmatrix} \mathbf{0} & \boldsymbol{I} \\ -\boldsymbol{M_s}^{-1}\boldsymbol{K_s} & -\boldsymbol{M_s}^{-1}\boldsymbol{C_s} \end{bmatrix}; \\ \boldsymbol{B} &= \begin{bmatrix} \mathbf{0} \\ \boldsymbol{M_s}^{-1}\boldsymbol{\Lambda} \end{bmatrix}; \qquad \boldsymbol{E} = \begin{bmatrix} \mathbf{0} \\ -\boldsymbol{l} \end{bmatrix} \end{aligned} \quad (3)$$

The output $\mathbf{y}(t)$ is the absolute acceleration at each floor; therefore, the matrices $\mathbf{C}$ and $\mathbf{D}$ are

$$\boldsymbol{C} = [-\boldsymbol{M_s}^{-1}\boldsymbol{K_s} \quad -\boldsymbol{M_s}^{-1}\boldsymbol{C_s}]; \quad \boldsymbol{D} = \left[\boldsymbol{M_s}^{-1}\boldsymbol{\Lambda}\right] \quad (4)$$

If the shear building is assumed with proportional damping, the equation of motion (Eq. (1)) can be transformed into the modal configuration by letting $\mathbf{x}(t) = \boldsymbol{\Phi}\boldsymbol{q}(t)$ as

$$\ddot{\boldsymbol{q}}(t) + \bar{\boldsymbol{C}}\dot{\boldsymbol{q}}(t) + \boldsymbol{\Omega}^2\boldsymbol{q}(t) = -\boldsymbol{\Phi}^T\boldsymbol{M_s}\boldsymbol{l}\ddot{x}_g(t) + \boldsymbol{\Phi}^T\boldsymbol{\Lambda}u(t) \quad (5)$$

where $\boldsymbol{\Phi}$ is $n \times n$ modal matrix which contains all the mode shapes; $\mathbf{q}(t)$ is a $n \times 1$ modal relative displacement vector; $\bar{\boldsymbol{C}} = diag(2\zeta_1\omega_1 \ \ 2\zeta_2\omega_2 \ \ \cdots \ \ 2\zeta_n\omega_n)$ is a $n \times n$ modal damping matrix in which the parameters ζ_i and ω_i represent the damping ratio and natural frequency of the ith mode, respectively ; and $\boldsymbol{\Omega}^2 = diag(\omega_1^2 \ \ \cdots \ \ \omega_n^2)$ is a $n \times n$ modal natural frequency matrix. If the modal states are defined as $\boldsymbol{z_m}(t) = [\boldsymbol{q}(t)\ \dot{\boldsymbol{q}}(t)]^T$, the state-space formulation of the structure in modal configuration can be represented as

$$\begin{aligned} \dot{\boldsymbol{z}}_{\boldsymbol{m}}(t) &= \boldsymbol{A_m}\boldsymbol{z_m}(t) + \boldsymbol{B_m}u(t) + \boldsymbol{E_m}\ddot{x}_g(t) \\ \boldsymbol{y_m}(t) &= \boldsymbol{C_m}\boldsymbol{z_m}(t) + \boldsymbol{D_m}u(t) \end{aligned} \quad (6)$$

where the system matrix $\mathbf{A_m}$, the control force distribution matrix $\mathbf{B_m}$, and the disturbance location matrix $\mathbf{E_m}$ in modal configuration are

$$\boldsymbol{A_m} = \begin{bmatrix} \mathbf{0} & \boldsymbol{I} \\ -\boldsymbol{\Omega}^2 & -\bar{\boldsymbol{C}} \end{bmatrix}; \quad \boldsymbol{B_m} = \begin{bmatrix} \mathbf{0} \\ \boldsymbol{\Phi}^T\boldsymbol{\Lambda} \end{bmatrix}; \quad \boldsymbol{E_m} = \begin{bmatrix} \mathbf{0} \\ -\boldsymbol{\Phi}^T\boldsymbol{M_s}\boldsymbol{l} \end{bmatrix} \quad (7)$$

Similarly, the output $\mathbf{y_m}(t)$ is the modal absolute acceleration of each mode and the matrices $\mathbf{C_m}$ and $\mathbf{D_m}$ are

$$\boldsymbol{C_m} = [-\boldsymbol{\Omega}^2 \quad -\bar{\boldsymbol{C}}]; \qquad \boldsymbol{D_m} = [\boldsymbol{\Phi}^T\boldsymbol{\Lambda}] \quad (8)$$

2.2 LQR control

LQR control method aims to minimize a cost function relating to the states and control inputs of the system with weighting matrices **Q** and **R** selected by users. Generally, a quadratic cost function of LQR for structural control is defined as

$$J = \int_0^\infty (\boldsymbol{z}^T \boldsymbol{Q} \boldsymbol{z} + u^T R u) dt \quad (9)$$

The state feedback gain matrix $\mathbf{K_g}$ is designated to form the control input $u(t) = -\mathbf{K_g} \boldsymbol{z}(t)$. In this study, the modal absolute acceleration is taken as the state to be regulated. Therefore, the cost function is modified with respect to the modal absolute acceleration as

$$J = \int_0^\infty (\boldsymbol{y_m}^T \boldsymbol{Q} \boldsymbol{y_m} + u^T R u) dt \quad (10)$$

Noted that the dimension of the weighting matrix **Q** can be greatly reduced by applying LQR modal control depending on the number of modes selected for control. The state feedback gain matrix $\mathbf{K_m}$ can be obtained by solving the Ricatti equation

$$\boldsymbol{K_m} = R^{-1} \boldsymbol{B_m}^T \boldsymbol{P} \quad (11)$$

where **P** is the solution of the Ricatti equation

$$\boldsymbol{A_m}^T \boldsymbol{P} + \boldsymbol{P} \boldsymbol{A_m} - \boldsymbol{P} \boldsymbol{B_m} R^{-1} \boldsymbol{B_m}^T \boldsymbol{P} + \boldsymbol{C_m}^T \boldsymbol{Q} \boldsymbol{C_m} = \boldsymbol{0} \quad (12)$$

The control input $u(t) = -\mathbf{K_m} \mathbf{z_m}(t)$ in modal space can be obtained. In order to convert the control input from the modal space to the configuration space, the gain matrix $\mathbf{K_m}$ needs to be transformed through the mode shape matrix as

$$\boldsymbol{K_g} = \boldsymbol{K_m} \begin{bmatrix} \boldsymbol{\Phi}^{-1} & \boldsymbol{0} \\ \boldsymbol{0} & \boldsymbol{\Phi}^{-1} \end{bmatrix} \quad (13)$$

Consequently, the state feedback gain matrix $\mathbf{K_g}$ can be used to control the structure in practice.

3. Optimization setting

Selecting the most proper weighting matrices for LQR is typically done by trial and error that is based on engineering sense and experience; however, the corresponding control performance may not be optimized. SOS was applied to optimize the weighting matrices of LQR with respect to a specified objective function. Noted that the dimension of weighting matrices can be significantly reduced in modal LQR control depending on the number of modes to be controlled as mentioned previously. In the optimization process, the selected number of the first modes depends on the condition that the corresponding accumulated effective modal mass is larger than 95% of the total structural mass. Furthermore, the magnitude of weightings in **Q** and R in Eq. (10) are relative. As a result, the number of weightings to be optimized is reduced to the number of control modes by assuming a fixed value of R and a diagonal matrix of **Q**.

3.1 Symbiotic organisms search

Symbiotic Organisms Search (SOS) is a metaheuristic optimization algorithm that emulates the biological interaction between two organisms in an ecosystem. It is noted that specific algorithm parameters are not required for SOS, providing a main advantage against other metaheuristic algorithms such as GA and PSO. There are three phases in SOS, namely mutualism phase, commensalism phase, and parasitism phase. The flowchart of SOS procedure is depicted in Fig. 1. In SOS, each organism is assigned random location in the N^{th} dimensional search space in the initialization process, and the fitness of each organism is evaluated subsequently. The location of the organism that has the best fitness value is recorded as $\mathbf{x_{best}}$. In the mutualism phase, two organisms are randomly selected. The position of each organism is then updated by using the equation defined as

$$\boldsymbol{x_{inew}} = \boldsymbol{x_i} + rand(0,1) \cdot (\boldsymbol{x_{best}} - \frac{\boldsymbol{x_i} + \boldsymbol{x_j}}{2} \cdot BF_1) \quad (14)$$

$$\boldsymbol{x_{jnew}} = \boldsymbol{x_j} + rand(0,1) \cdot (\boldsymbol{x_{best}} - \frac{\boldsymbol{x_i} + \boldsymbol{x_j}}{2} \cdot BF_2) \quad (15)$$

where $\mathbf{x_{inew}}$ and $\mathbf{x_{jnew}}$ are the new position of the i^{th} and j^{th} organisms, respectively; and BF_1 and BF_2 are benefit factors of the i^{th} and j^{th} organisms, respectively. Noted that BF_1 and BF_2 are determined randomly as either 1 or 2 at each iteration step which represent the benefit level to individual organism. In other words, BF_1 and BF_2 are utilized to simulate the interaction of two organisms whether one of them partially or fully benefits from the other. Therefore, tuning of BF_1 and BF_2 is not required in SOS. Finally, $\mathbf{x_{best}}$ is updated by the new position of the organism as long as the new fitness is better than the pre-interaction fitness. The commensalism phase is conducted after the mutualism phase is completed. Similar to the mutualism phase, two organisms are selected. One of the two organisms intends to get benefit from the other by updating its position as

$$\boldsymbol{x_{inew}} = \boldsymbol{x_i} + rand(-1,1) \cdot (\boldsymbol{x_{best}} - \boldsymbol{x_j}) \quad (16)$$

If the obtained fitness by the new positon is better than the previous fitness, then $\mathbf{x_{best}}$ is updated by the new position of the organism. Subsequently, it turns to the parasitism phase in which a parasite organism is created by duplicating a randomly-selected organism and modifying the organism with a generated random number. Then, another organism is selected randomly as the host to be attacked. The fitness values of the parasite and the host are evaluated. If the parasite has a better fitness value, it kills the host organism and assumes its position in the ecosystem. On the contrary, if the parasite does not have a better fitness value, it is terminated immediately. If the fitness is better than the previous best fitness in the ecosystem, then $\mathbf{x_{best}}$ is updated by the new position of the parasite organism. The mutualism, commensalism, and parasitism phases work in a loop until the predefined number of iteration steps is reached.

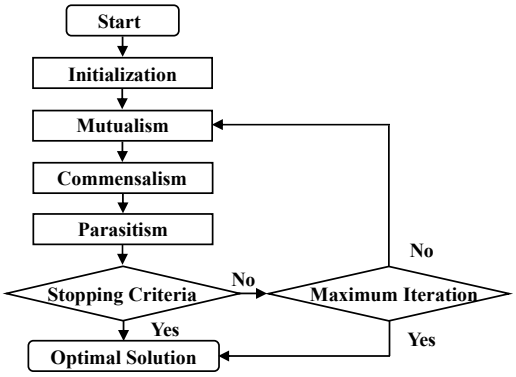

Fig. 1 Symbiotic organisms search flowchart

3.2 Objective functions

Defining the objective function is the key factor for metaheuristic optimization algorithms. An appropriate objective function leads to satisfactory seismic performance in structural control. In this study, the main control target is aimed to reduce the acceleration response of the benchmark structure subjected to earthquakes. Accordingly, three objective functions with respect to the modal configuration are proposed and minimized by applying SOS algorithm. In Eq. (6), the modal absolute acceleration $\mathbf{y_m}(t)$ has a dimension of $n_m \times 1$ at each time step if merely the first n_m modes are considered. Let $a_m(t)$ be the sum of the n_m elements at each time step, and $y_{mi}(t)$ be the i^{th} element of $\mathbf{y_m}(t)$, the three objective functions proposed in this study can be defined as

$$\text{OBJ1} = \sqrt{\frac{\sum_{k=1}^{n_t} a_m(k\Delta t)^2}{n_t}} \tag{17}$$

$$\text{OBJ2} = \max_{k=1\cdots n_t} |a_m(k\Delta t)| \tag{18}$$

$$\text{OBJ3} = \sqrt{\max_{k=1\cdots n_t} [y_{m1}(k\Delta t)^2] + \max_{k=1\cdots n_t} [y_{m2}(k\Delta t)^2] + \cdots + \max_{k=1\cdots n_t} \left[y_{mn_m}(k\Delta t)^2\right]} \tag{19}$$

where Δt is the sampling period and n_t is the number of samples. Apparently, OBJ1 and OBJ2 represent the root-mean-square (RMS) and maximum of the sum of modal absolute acceleration of the first n_m control modes, respectively; and OBJ3 concerns the square root of the sum of the squares (SRSS) of the maximum modal absolute acceleration of the first n_m control modes.

3.3 Benchmark structure

A 10-story shear building used by Amini *et al*. (2013) was adopted to evaluate the optimizing performance of SOS with respect to the three objective functions introduced before. The mass and the stiffness of each story were 10 kN-s^2/m and 2,000 kN/m, respectively. The undamped natural frequencies of the structure are shown in Table 1. It was assumed that an active mass damper was installed on the top floor of the structure with a force capacity of ±50 kN which was approximately equal to 5% total weight of the structure. A schematic of the structure with AMD is depicted in Fig. 2. The damping ratio of the structure was assumed 2% for all modes. In order to determine the number of modes (n_m) to be controlled, the effective modal mass was adopted which provides an approach for evaluating the significance of a vibration mode. In the study, the total effective modal mass of the first n_m modes has to be larger than 95% of the actual mass. The effective modal mass of the 1st, 2nd, and 3rd mode was 84.79 kN-s^2/m, 9.14 kN-s^2/m, and 3.09 kN-s^2/m, respectively. Therefore, merely the first three modes were adopted for control in the numerical simulation (n_m = 3).

3.4 Force saturation

Saturation is commonly applied in numerical simulation to emulate an actuation device that exceeds its capacity by sustaining its peak quantity (Pnevmatikos and Gantes 2011). Such limitation must be properly considered because the control device exerts large control force on which may lead to damages of the control system and inferior control effectiveness (BrazCésar and Barros 2018). In addition, the tradeoff between economy and performance was also considered in the optimization by applying saturation as the control force was not unlimited. Noted that the force capacity of the actuator used in the AMD was assumed 5% of the structural weight. Instead of applying saturation of full actuator force capacity, saturation with 10% of the actuator capacity (±5 kN) was used. This is because the weightings in **Q** matrix blew up which resulted in extremely huge control force in the optimization process. In this

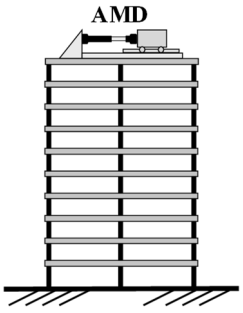

Fig. 2 Schematic of the 10-story benchmark shear building controlled by an AMD

Table 1 Natural frequencies of the 10-story building (rad/sec)

Mode	1	2	3	4	5	6	7	8	9	10
Natural frequency	2.11	6.29	10.33	14.14	17.64	20.73	23.37	25.48	27.03	27.97

manner, step-like control force could be generated and imposed on the structure which should be avoided in real practice. In addition, the advantage of applying 10% saturation was that it reduced the search field of metaheuristic algorithms which made the optimization process accelerated. Furthermore, the generated control force can be close to the force capacity of actuation device if the 10% force saturation is considered in the optimization process. After optimization process was completed, the saturation of 10% actuator capacity was replaced by saturation of 100% actuator capacity to evaluate the control performance.

4. Numerical simulation

MATLAB/Simulink was used to perform the numerical simulation of the 10-story benchmark structure with AMD optimized by SOS with respect to the three proposed objective functions. The weighting R was set to a fixed value of 100. Meanwhile, 10^5 and 0 were used as the upper and lower bounds value for $\mathbf{Q}$. Saturation block provided by Simulink library was utilized to ensure that the control force was bounded to the upper and lower saturation values.

4.1 Performance indices

In the numerical simulation, four of the performance indices used by Jansen and Dyke (2000) were adopted to evaluate the control performance of the AMD based on different objective functions. The first performance index denotes the maximum normalized floor relative displacement which can be expressed as

$$J_1 = \max_{t,i}\left(\frac{|x_i(t)|}{x^{\max}}\right) \tag{20}$$

where $x_i(t)$ is the relative displacement of the i^{th} floor during the excitation; and $x^{\max}$ represents the maximum displacement of the uncontrolled shear building. The second performance index is the maximum normalized inter-story drift which can be represented as

$$J_2 = \max_{t,i}\left(\frac{|d_i(t)/h_i|}{{d_n}^{\max}}\right) \tag{21}$$

where $d_i(t)$ is the inter-story drift of the i^{th} floor during the excitation; h_i is the story height of the i^{th} floor; and ${d_n}^{\max}$ represents the maximum normalized inter-story drift of the uncontrolled shear building. The third performance index is the normalized peak absolute acceleration which can be expressed as

$$J_3 = \max_{t,i}\left(\frac{|\ddot{x}_{ai}(t)|}{{\ddot{x}_{ai}}^{\max}}\right) \tag{22}$$

where $\ddot{x}_{ai}(t)$ is the absolute acceleration of the i^{th} floor during the excitation; and ${\ddot{x}_{ai}}^{\max}$ is the maximum absolute acceleration of the i^{th} floor of the uncontrolled shear building. The last performance index considers the maximum control force normalized by the weight of the structure

$$J_4 = \max_{t}\left(\frac{|u(t)|}{W}\right) \tag{23}$$

where $u(t)$ is the control force of AMD and W is the weight of the 10-story benchmark structure.

4.2 Optimization results

4.2.1 Superiority of SOS

The first stage was to compare the optimization results of SOS with those of other optimization algorithms. Two common optimization methods including genetic algorithm (GA), and particle swarm optimization (PSO) were applied to this benchmark structure for comparison purposes. Noted that the benchmark structure was represented by a linear time-invariant system without considering modeling error and uncertainty for simplicity purpose. Therefore, the optimization results obtained from different optimization methods can be investigated in a direct and clear manner. It is known that the seismic response of a structure is dependent on the characteristics of ground motion such as frequency components, intensity, and duration. For the purpose of generality, the 10-story benchmark structure was excited by a band-limited white noise (BLWN) ground acceleration with a root-mean-square of 1 m/s^2, a bandwidth from 0 Hz to 20 Hz, and a duration of 40 seconds. As mentioned previously, R was set to a fixed value of 100, and $\mathbf{Q}$ was optimized by the three metaheuristic algorithms with an upper bound and a lower bound of 10^5 and 0, respectively. All the three metaheuristic algorithms used 100 individuals (chromosomes for GA, particles for PSO, and organisms for SOS) for optimization. However, 35 iterations were adopted for SOS while 100 iterations were conducted for GA and PSO considering SOS contained three phases. For the setting of GA tuning parameters, the crossover and mutation rate were set 0.8, and 0.1, respectively. For the setting of PSO tuning parameters, c_1 and c_2 were set 4.0. Fig. 3 shows the mean optimization results of 20 trials for each optimization algorithms with respect to the three objective functions. It can be seen that SOS permanently obtains the minimum objective function reduction compared to the other two algorithms. Table 2 shows the standard deviation of the 20 trials of the three optimization algorithms with respect to the three objective functions. It demonstrates that SOS achieves better robust optimization performance against random bias than the other two optimization algorithms. Moreover, SOS has an advantage that it does not need to define any optimization parameter in the algorithm. In other words, SOS does not need to conduct trial and error method to determine the best optimization parameter in the algorithm. On the contrary, GA needs to define the crossover and mutation parameters to obtain proper optimization result, and PSO needs to define the inertia weight, and acceleration constants in order to achieve good optimization performance. Herein, SOS performs the best among the three algorithms regarding the optimization results as well as the simplicity of application. Averagely speaking, in term of the rate of convergence of the 20 trials, GA and PSO start to converge at the 49$^{\text{th}}$ and 22$^{\text{nd}}$ iteration, respectively while SOS starts to converge at the 6$^{\text{th}}$ iteration for OBJ1. For OBJ2, GA and PSO started to

Table 2 Standard deviation of the 20 trials for each optimization algorithm with the three objective functions

Optimization algorithm	GA			PSO			SOS		
Objective function	OBJ1	OBJ2	OBJ3	OBJ1	OBJ2	OBJ3	OBJ1	OBJ2	OBJ3
Standard deviation	0.114	0.836	0.288	0.134	0.250	0.114	$6.17e^{-5}$	$3.58e^{-4}$	$2.31e^{-4}$

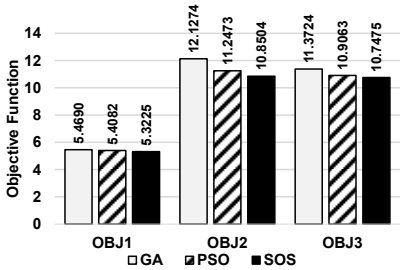

Fig. 3 Mean optimization results of three algorithms with respect to the objective functions

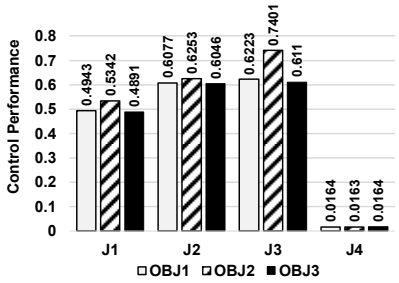

Fig. 4 Optimization results of objective functions with respect to the performance indices

converge at the 50th and 33rd iteration, respectively while SOS started to converge at 28th iteration. Lastly for OBJ3, GA and PSO started to converge at the 52nd and 43rd iteration, respectively while SOS started to converge at the 18th iteration. As a result, the rate of convergence of SOS is better than the other two optimization algorithms.

4.2.2 Performance of objective functions

The control performance indices were used to determine the best objective function. Since SOS was superior to GA and PSO with respect to the three objective functions as shown previously, SOS was adopted as the optimization algorithm for the subsequent simulation. Fig. 4 shows the simulation results of the three objective functions in terms of the performance indices. It can be found that the control performance of OBJ3, which concerns the SRSS of the maximum modal absolute acceleration is superior than the other two objective functions. As a result, it can be concluded that OBJ3 is the finest among the three objective functions.

4.2.3 Saturation effect

As mentioned previously, saturation with 10% of the actuator capacity of AMD was used in the optimization process. Without this 10% saturation during the optimization of the weighting matrices, the generated force of the LQR controller could reach the force capacity of the

Table 3 Four control cases considering the saturation effect

Case number	1	2	3	4
Saturation level/ Force capacity	10%	100%	100%	100%
Control force adjusting method	None	Increase *R*	Apply gain	None

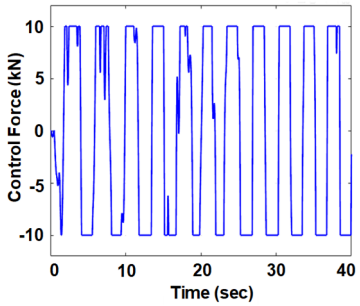

Fig. 5 Step-like control force

AMD actuator, leading to step-like control force as shown in Fig. 5 which could deteriorate the control performance of the AMD control system. However, the control force can be adjusted by applying a gain smaller than 1.0 or increasing the *R* value in the cost function for smaller control force. In order to realize the saturation effect, four LQR control cases were considered as documented in Table 3. In the optimization process, a BLWN with a bandwidth from 0 Hz to 20 Hz, a peak ground acceleration of 2.4 m/s^2, and a duration of 140 seconds was adopted as the excitation input to the 10-story benchmark structure. The four cases were all optimized by applying SOS with the objective function of OBJ3. The maximum control force in Case 2 to 3 was adjusted to the identical level of Case 1 for comparison purposes. Fig. 6 shows the optimization results of the four cases in terms of the performance indices. It can be found that Case 4 performs worse than Case 1, indicating that step-like control force results in unfavorable control performance. In particular, the control performance of Case 4 is even worse than that of the uncontrolled building regarding maximum displacement of the building. After reducing the control force by either increasing *R* in the cost function (Case 2) or applying a gain smaller than 1.0 (Case 3), the corresponding control performance of the two cases is extremely diverse. Case 2 has approximately identical control performance as Case 1 does; however, Case 3 has the worst control performance among the four cases which even enlarges the seismic performance of the shear building. As a result, it is suggested that two approaches can be applied for the optimization process of weighting matrices. The first one is to apply 10% saturation of force

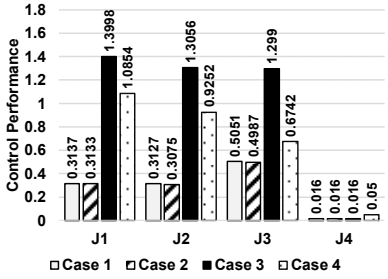

Fig. 6 Optimization results of four cases considering the effect of saturation

capacity during the optimization process and directly use the optimized weighting matrices of LQR for practical control. The other one is to apply 100% saturation of force capacity during the optimization process and adjust the control force level by increasing R value for practical control.

4.3 Seismic control performance

Fourteen earthquake ground acceleration records normalized to a PGA of 0.24 g, which is the design basis earthquake in Taipei basin, were used as the ground excitation to the 10-story benchmark structure. The weighting matrices of the LQR controller were optimized by applying SOS with OBJ3 objective function to generate the control force of the AMD. For optimization of the weighting matrix $\mathbf{Q}$, the bandwidth of the BLWN was altered from 0-20 Hz to 0-15 Hz as simulation results indicated that they provided approximate identical control performance. A narrow bandwidth of excitation was helpful to concentrating the control force on the first three modes of the 10-story shear building. Besides, a bandwidth of 0-15 Hz was able to cover the frequency component of most of the historical earthquake records whose amplitude above 15 Hz is insignificant and thus can be neglected. During the optimization process, 10% saturation of the force capacity of the AMD actuator was also applied. Meanwhile, 20 trials of SOS were conducted to eliminate the random bias and the one with the least OBJ3 value was adopted for the seismic simulation. Table 4 lists the performance indices of the 10-story building with AMD subjected to the fourteen earthquakes. Averagely speaking, more than 30% of the seismic response of the building was mitigated with merely 3% control force of the building weight.

In order to demonstrate the control effectiveness of the automatic tuning method of the weighting matrices using SOS, three additional common weighting matrix tuning methods mentioned by Alavinasab *et al.* (2006) were applied for comparison purposes. These methods consider the variant of the $\mathbf{Q}$ matrix in LQR. In this study, the variant of these $\mathbf{Q}$ matrices is named method 1 to 3 and can be represented as

$$\boldsymbol{Q_1} = 10^{q_i}\begin{bmatrix}\boldsymbol{K_s} & \boldsymbol{0}\\ \boldsymbol{0} & \boldsymbol{M_s}\end{bmatrix};\quad \boldsymbol{Q}_2 = 10^{q_i}\begin{bmatrix}\boldsymbol{I} & \boldsymbol{0}\\ \boldsymbol{0} & \boldsymbol{0}\end{bmatrix};\quad \boldsymbol{Q}_3 = 10^{q_i}\begin{bmatrix}\boldsymbol{I} & \boldsymbol{0}\\ \boldsymbol{0} & \boldsymbol{I}\end{bmatrix} \tag{24}$$

where q_i is the parameter for tuning. Noted that R = 1.0 was used for all cases. The parameter q_i for each method was determined by trial and error based on the objective that the generated maximum control force was approximate to the maximum control force of the proposed tuning method, which was 3% structural weight as shown in Table 4. Noted that the weighting matrix $\mathbf{Q_1}$ (method 1) was related to a factored combination of strain energy and kinetic energy of the structural therefore, method 1 was also called energy-based method. Accordingly, q_i was selected as 1.525, 3.525, and 2.710 for $\mathbf{Q_1}$, $\mathbf{Q_2}$, and $\mathbf{Q_3}$, respectively. The performance indices of the 10-story building with AMD controlled by LQR with the weighting matrix $\mathbf{Q_1}$, $\mathbf{Q_2}$, and $\mathbf{Q_3}$ subjected to the fourteen earthquakes are shown in

Table 4 Seismic control performance of the SOS optimization method for LQR weightings

Earthquakes	J_1	J_2	J_3	J_4
Chi-Chi	0.472	0.814	0.690	0.016
Kumamoto	0.543	0.718	0.648	0.020
Imperial Valley	0.553	0.531	0.606	0.040
Kobe	0.531	0.584	0.645	0.029
Chuetsu Oki	0.605	0.549	0.674	0.030
Meinong	0.686	0.747	0.655	0.049
Northridge	0.553	0.655	0.895	0.025
Parkfield	0.702	0.797	0.732	0.022
El-Centro	0.434	0.523	0.803	0.020
Montenegro	0.778	0.812	0.701	0.030
Capemendocino	0.557	0.677	0.684	0.028
El-Mayor	0.584	0.618	0.569	0.030
Darfield	0.846	0.896	0.744	0.033
TPA-013	0.501	0.487	0.462	0.047
Average	0.596	0.672	0.679	0.030

Table 5 Seismic control performance of the tuning method 1 for LQR weightings ($\mathbf{Q_1}$)

Earthquakes	J_1	J_2	J_3	J_4
Chi-Chi	0.418	0.908	0.820	0.012
Kumamoto	0.435	0.604	0.652	0.022
Imperial Valley	0.441	0.493	0.551	0.047
Kobe	0.465	0.623	0.750	0.020
Chuetsu Oki	0.485	0.506	0.746	0.029
Meinong	0.587	0.757	0.808	0.041
Northridge	0.510	0.657	0.863	0.030
Parkfield	0.734	0.871	0.855	0.022
El-Centro	0.371	0.619	0.899	0.024
Montenegro	0.753	0.766	0.853	0.036
Capemendocino	0.513	0.707	0.835	0.022
El-Mayor	0.485	0.768	0.683	0.033
Darfield	0.726	0.859	0.700	0.033
TPA-013	0.446	0.485	0.591	0.050
Average	0.526	0.687	0.758	0.030

Table 6 Seismic control performance of the tuning method 2 for LQR weightings ($\mathbf{Q}_2$)

Earthquakes	J_1	J_2	J_3	J_4
Chi-Chi	0.501	1.087	0.949	0.017
Kumamoto	0.413	0.579	0.721	0.023
Imperial Valley	0.419	0.524	0.671	0.053
Kobe	0.451	0.749	0.889	0.018
Chuetsu Oki	0.447	0.535	0.984	0.031
Meinong	0.547	0.780	1.038	0.045
Northridge	0.510	0.659	1.005	0.028
Parkfield	0.788	1.017	1.063	0.023
El-Centro	0.382	0.772	1.267	0.025
Montenegro	0.756	0.807	1.022	0.040
Capemendocino	0.513	0.775	1.193	0.028
El-Mayor	0.523	0.979	1.042	0.026
Darfield	0.669	0.856	0.894	0.033
TPA-013	0.489	0.598	0.841	0.055
Average	0.529	0.766	0.970	0.032

Table 7 Seismic control performance of the tuning method 3 for LQR weightings ($\mathbf{Q}_3$)

Earthquakes	J_1	J_2	J_3	J_4
Chi-Chi	0.430	0.932	0.833	0.012
Kumamoto	0.441	0.610	0.655	0.021
Imperial Valley	0.449	0.484	0.567	0.046
Kobe	0.478	0.632	0.769	0.019
Chuetsu Oki	0.496	0.504	0.768	0.027
Meinong	0.592	0.750	0.820	0.039
Northridge	0.511	0.657	0.871	0.028
Parkfield	0.745	0.900	0.879	0.021
El-Centro	0.383	0.627	0.937	0.023
Montenegro	0.749	0.749	0.865	0.034
Capemendocino	0.524	0.702	0.867	0.022
El-Mayor	0.495	0.790	0.714	0.032
Darfield	0.738	0.851	0.722	0.033
TPA-013	0.448	0.509	0.614	0.049
Average	0.534	0.693	0.777	0.029

Table 5, 6, and 7, respectively. It can be clearly observed that the control performance of the proposed automatic tuning method outperforms that of the three methods in terms of J_2 and J_3. However, the control performance of the three methods provide better results compared to the proposed tuning method in terms of J_1. It is because the cost function to be minimized for the three tuning methods was related to the structural states, i.e., the displacement and velocity. The performance index J_1 considers the maximum normalized floor relative displacement. Therefore, it is acceptable that the proposed automatic tuning method had inferior performance on J_1. Nevertheless, the three tuning methods tend to merely suppress the relative displacement while the proposed tuning method provides balanced control performance regarding story drift and acceleration.

5. Experimental validation

5.1 Experimental setup

The seismic performance of a structure with AMD controlled by the LQR with the proposed SOS optimization method of weighting matrices was further investigated by conducting shake table testing in the small-scale structural laboratory located in National Center for Research on Earthquake Engineering (NCREE) in Taipei, Taiwan (Chen *et al*. 2020). The experimental setup is depicted in Fig. 7. A SDOF shear building model with a weight of 450 N was fixed on a shake table. The AMD installed on the top of the building model was composed of an AC motor, a guide screw, and a mass block. The AC motor was controlled by an analog controller which converted an input voltage into a current output; therefore, and the torque of the motor was controlled by the current output. The weight of the mass block was 20 N, which was 4.4% weight of the shear building model. Three high-resolution MEMS accelerometers manufactured by Silicon Designs, Inc. were used in the experimental validation. One was installed on the bottom rigid plate connected to the shake table to record the reproduced ground motions; one was installed on the roof of the building model to measure the corresponding absolute acceleration; and the last one was installed on the mass block to convert the control force from the measured acceleration. The maximum input acceleration range of each accelerometer was ±2 g. Meanwhile, a Temposonics GH linear-position sensor was installed between the roof and the platen of shake table to measure the relative displacement of the shear building. Noted that the states for feedback control in the experimental validation were not fully measurable; therefore, a Kalman filter was designed for estimating the states of the shear building, making the LQR become a linear-quadratic-Gaussian (LQG) controller. The shake table was driven by a dynamic servo-hydraulic actuator with maximum stroke and force capacity of ±127 mm and ±15 kN, respectively. The dimension of the shake table rigid platen made of aluminum was 1000 mm × 800 mm. An MTS FlexTest® Controller FT-100 digital controller was used to control the actuator using a propor-

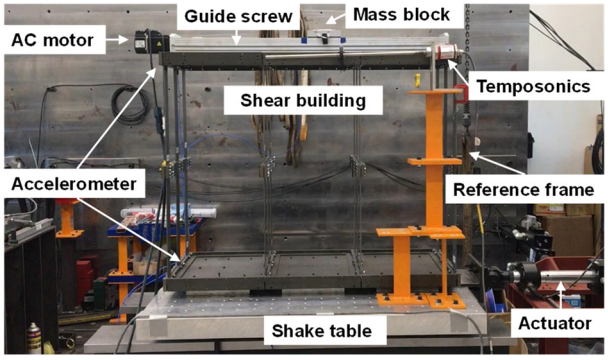

Fig. 7 Experimental setup for the validation

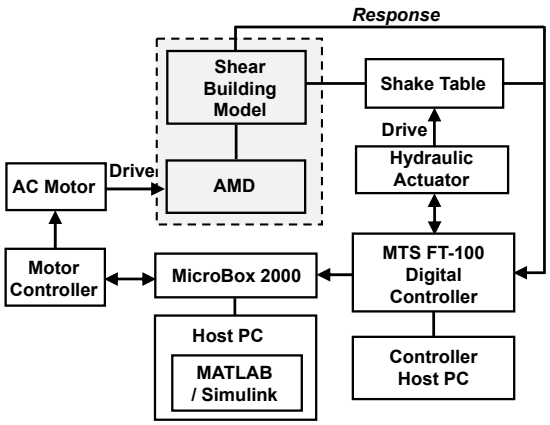

Fig. 8 Hardware and software layout for the experimental validation

tional-integral-derivative control loop. In addition, a Micro-Box 2000 developed by TeraSoft Inc. was adopted to implemented the LQG for structural control which provided multi-function platform for rapid control prototyping applications. The LQG was built on the host PC using MATLAB/Simulink and connected to I/O hardware with blocks provided by Simulink Real-Time. Executable C-code was compiled and downloaded onto the Micro-Box 2000 to run the control application. The hardware and software layout for the experimental validation is depicted in Fig. 8.

5.2 Experimental results

Before designing the LQG for the AMD, the structural properties of the SDOF shear building model were identified first. The natural frequency and damping ratio of the model were 0.905 Hz and 0.25%, respectively. The LQG was designed based on the identified SDOF structural model and the modeling error was considered insignificant. Two tuning methods of the LQG weighting matrices were processed for comparison purposes including the proposed SOS optimization approach and the energy-based tuning method (method 1). Due to the fact that the natural frequency of the shear building model was 0.905 Hz, the stroke limitation of the AMD could restrict the control force level applied to the structure. Therefore, the aforementioned fourteen earthquake ground acceleration records were normalized to a PGA of 0.8 m/s^2 in the experimental

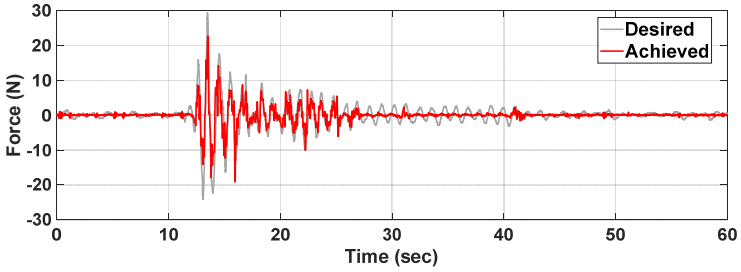

Fig. 9 Time histories of the desired and achieved force of AMD under Kobe earthquake

Table 8 Seismic control performance of the validating tests

	Proposed method (SOS + OBJ3 +10% saturation)			Energy-based method (method 1)		
Earthquakes	J_1 and J_2	J_3	J_4	J_1 and J_2	J_3	J_4
Chi-Chi	0.617	0.760	0.034	0.584	0.787	0.030
Kumamoto	0.557	0.661	0.020	0.610	0.680	0.024
Imperial Valley	0.541	0.599	0.028	0.546	0.716	0.025
Kobe	0.484	0.587	0.052	0.529	0.621	0.050
Chuetsu Oki	0.778	0.811	0.034	0.673	0.843	0.030
Meinong	0.614	0.567	0.045	0.586	0.646	0.044
Northridge	0.778	0.819	0.038	0.682	0.860	0.033
Parkfield	0.390	0.415	0.047	0.359	0.363	0.041
El-Centro	0.399	0.460	0.046	0.387	0.557	0.040
Montenegro	0.631	0.628	0.051	0.569	0.597	0.036
Capemendocino	0.753	0.744	0.051	0.674	0.842	0.033
El-Mayor	0.545	0.549	0.038	0.571	0.633	0.041
Darfield	0.631	0.522	0.037	0.602	0.682	0.043
TPA-013	0.611	0.523	0.032	0.619	0.628	0.041
Average	0.595	0.618	0.039	0.571	0.675	0.037

validation in order to reduce the control force demand for the AMD. Meanwhile, friction force between the guide screw and the mass block was observed during the tests which affected the control performance of the AMD. Thus, friction compensation was applied to the motor control voltage for accurately controlling the AMD. Fig. 9 shows the desired and achieved force time histories of the AMD when the shear building model was subjected to the Kobe ground motion. The desired force in Fig. 9 was calculated by the proposed tuning method of LQG. The achieved force was obtained by multiplying the mass by the measured acceleration of the mass block. Apparently, the AMD was able to track the desired force fairly well after applying the friction compensation. Table 8 lists the performance indices of each validating test. Noted that J_1 and J_2 were identical in the validating tests as the shear building model was merely single degree-of-freedom. It can be observed that the proposed metaheuristic optimization method suppressed the structural acceleration response more than the energy-based tuning method did under a similar control force level. Averagely speaking, the acceleration response was suppressed 17% more by applying the proposed tuning method. On the other hand, the displacement response of the proposed tuning method was just 4% larger than the energy-based tuning method. Since the objective function for the optimization process was aimed to reduce the acceleration response of the structure, the results were expected and reasonable. Lastly, the objective function for SOS algorithm can be modified if further displacement response suppression is required, providing the engineers with flexible optimization of the LQG weighting matrices.

6. Conclusions

In this study, a novel metaheuristic optimization algorithm named symbiotic organisms search (SOS) was adopted for automatically optimizing the weighting matrices of LQR for structural control with an active mass damper (AMD). The SOS emulated the interactive behavior among organisms in nature with three phases, namely mutualism, commensalism, and parasitism. Modal control was used as the acceleration response of a structure was dominated by the first few modes. Three objective functions were proposed for optimization including the root-mean-square of the sum of modal acceleration, the maximum of the sum of modal acceleration, and the square root of the sum of the squares (SRSS) of the maximum modal absolute acceleration. Numerical simulation results indicated that the SOS achieved the minimum value of each objective function compared to the selected two common algorithms including the genetic algorithm (GA) and the particle sward optimization (PSO) in the 20 trials for each objective function. Meanwhile, SOS achieves robust optimization performance against random bias which can be observed from the standard deviation of the 20 trials. Besides, parameters setting was not required for SOS, leading to an effective and convenient auto-tuning of LQR weighting matrices. Furthermore, the rate of convergence of SOS was faster than that GA and PSO in average. The effect of AMD force saturation on the optimization process was also evaluated in this study. Four cases which considered the force limitation by applying either 10% or 100% saturation, as well as the force level by either applying a factor less than 1.0 or increasing the R value in the cost function. Numerical results indicated that two of the four cases were suggested in real practice. It was suggested to apply 10% saturation and the corresponding optimized weighting matrices was used directly. Alternatively, it was suggested to apply 100% saturation and adjust the control force level by increasing R. However, the former one was more straightforward to operate in real application since no further adjustment was needed. In summary, the proposed automatic tuning method adopted the SOS algorithm to optimize the SRSS of the maximum modal absolute acceleration considering the saturation effect. Afterwards, numerical simulation and experimental validation were conducted to realize the seismic control performance by using the proposed SOS tuning method of the LQR weighting matrices.

Fourteen historical earthquake ground motions were selected for both numerical and experimental studies. A 10-story benchmark structure was adopted for numerical simulation while a SDOF shear building model was designed and fabricated for experimental validation. The ground motions were normalized to a PGA of 0.24 g and 0.08 g for the numerical simulation and experimental validation, respectively. Three common weighting matrix tuning methods were adopted for comparison purposes in the numerical simulation among which the energy-based tuning method which considered a combination of strain energy and kinetic energy of the structure was further implemented in the experimental validation. The numerical results demonstrated that the proposed optimization method of LQR weighting matrices provided better seismic control performance regarding the floor acceleration and story drift. However, the floor relative displacement was slightly larger than the other three tuning methods. Similar results were observed in the experimental validation. Conclusively, the proposed automatic optimization method provides a simple and straightforward approach to determine the LQR weighting matrices for active structural control implementation. The numerical and experimental results demonstrate that the proposed tuning method achieves balanced control performance regarding story drift and acceleration.

Acknowledgments

The authors would like to express our sincere gratitude to the experimental facilities and expense supported by NCREE (06109A2500) as well as the financial support provided by the Taiwan Building Technology Center, National Taiwan University of Science and Technology from The Featured Areas Research Center Program within the framework of the Higher Education Sprout Project by the Ministry of Education in Taiwan.

References

Amini, F., Hazaveh, N.K. and Rad, A.A. (2013), "Wavelet PSO-based LQR algorithm for optimal structural control using active tuned mass dampers", *Comput.-Aided Civil Infrastruct. Eng.*, **28**(7), 542-557. https://doi.org/10.1111/mice.12017

Alavinasab, A., Moharrami, M. and Khajepour, A. (2006), "Active control of structures using energy-based LQR method", *Comput.-Aided Civil Infrastruct. Eng.*, **21**(8), 605-611. https://doi.org/10.1111/j.1467-8667.2006.00460.x

Bani-Hani, K.A. (2007), "Vibration control of wind-induced response of tall buildings with an active tuned mass damper using neural networks", *Struct. Control Health Monitor.*, **14**(1), 83-108. https://doi.org/10.1002/stc.85

Bhushan, R., Chatterjee, K. and Shankar, R. (2016), "Comparison between GA-based LQR and conventional LQR control method of DFIG wind energy system", *Proceedings of the 3rd International Conference on Recent Advances in Information Technology* (*RAIT*), March. Dhanbad, India.

Bozer, A. and Özsarıyıldız, Ş.S. (2018), "Free parameter search of multiple tuned mass dampers by using artificial bee colony algorithm", *Struct. Control Health Monitor.*, **25**(2), e2066. https://doi.org/10.1002/stc.2066

Braz-César, M.T. and Barros, R. (2018), "Semi-active fuzzy basedcontrol system for vibration reduction of a SDOF structure under seismic excitation excitation", *Smart Struct. Syst.*, *Int. J.*, **21**(4), 389-395. https://doi.org/10.12989/sss.2018.21.4.389

Cao, H. and Li, C. (2012), "Design of active tuned mass damper based on robust control", *IEEE International Conference on Computer Science and Automation Engineering* (*CSAE*), pp. 760-764.

Cao, H., Reinhorn, A.M. and Soong, T.T. (1998), "Design of active mass damper for a tall TV tower in Nanjing China", *Eng. Struct.*, **20**(3), 134-143. https://doi.org/10.1016/S0141-0296(97)00072-2

Çelik, E. and Durgut, R. (2018), "Performance enhancement of automatic voltage regulator by modified cost function and symbiotic organisms search algorithm", *Eng. Sci. Technol*, *Int. J.*, **21**(5), 1104-1111. https://doi.org/10.1016/j.jestch.2018.08.006

Chang, C.C. and Yang, H.T.Y. (1995), "Control of buildings using active tuned mass damper", *J. Eng. Mech.*, **121**(3), 355-366. https://doi.org/10.1061/(ASCE)0733-9399(1995)121:3(355)

Chen, Z. and Casciati, S. (2012), "An active mass damper system for structural control using real-time wireless sensors", *Struct. Control Health Monitor.*, **19**(8), 758-767. https://doi.org/10.1002/stc.1485

Chen, C.J. and Yang, S.M. (2014), "Application neural network controller and active mass damper in structural vibration suppression", *J. Intell. Fuzzy Syst.*, **27**, 2835-2845. https://doi.org/10.3233/IFS-141245

Chen, P.C., Ting, G.C. and Li, C.H. (2020), "A versatile small-scale structural laboratory for novel experimental earthquake engineering", *Earthq. Struct.*, *Int. J.*, **18**(3), 337-348. https://doi.org/10.12989/eas.2020.18.3.337

Cheng, M.Y. and Prayogo, D. (2014), "Symbiotic organisms search: A new metaheuristic optimization algorithm", *Comput. Struct.*, **139**, 98-112. https://doi.org/10.1016/j.compstruc.2014.03.007

Duan, H. and Sun, C. (2013), "Pendulum-like oscillation controller for micro aerial vehicle with ducted fan based on LQR and PSO", *Sci. China Technol. Sci.*, **56**(2), 423-429. https://doi.org/10.1007/s11431-012-5065-5

Dyke, S.J., Spencer, Jr. B.F., Quast, P., Kaspari, Jr. D.C. and Sain, M.K. (1996), "Implementation of an active mass driver using acceleration feedback control", *Microcomput. Civil Eng.*, **11**, 305-323. https://doi.org/10.1111/j.1467-8667.1996.tb00445.x

Jacknoon, A. and Abido, M.A. (2017), "Ant colony based LQR and PID tuned parameters for controlling inverted pendulum", *Proceedings of International Conference on Communication*, *Control*, *Computing and Electronics Engineering*, January, Khartoum, Sudan.

Jang, D.D., Jung, H.J. and Moon, Y.J. (2014), "Active mass damper system using time delay control algorithm for building structure with unknown dynamics", *Smart Struct. Syst.*, *Int. J.*, **13**(2), 305-318. https://doi.org/10.12989/sss.2014.13.2.305

Jansen, L.M. and Dyke, S.J. (2000), "Semiactive control strategies for MR dampers: comparative study", *J. Eng. Mech.*, **126**(8), 795-803. https://doi.org/10.1061/(ASCE)0733-9399(2000)126:8(795)

Kennedy, J. and Eberhart, R. (1995), "Particle swarm optimization", *Proceedings of ICNN'95 - International Conference on Neural Networks*, November-Deccember, Perth, WA, Australia.

Li, L., Wang, N. and Qin, H. (2019), "Adaptive model reference sliding mode control of structural nonlinear vibration", *Shock Vib.*, Article ID 3612516. https://doi.org/10.1155/2019/3612516

Lim, C.W. (2008), "Active vibration control of the linear structure with an active mass damper applying robust saturation controller", *Mechatronics*, **18**(8), 391-399. https://doi.org/10.1016/j.mechatronics.2008.06.006

Moghaddasie, B. and Jalaeefar, A. (2019), "Optimization of LQR method for the active control of seismically excited structures", *Smart Struct. Syst.*, *Int. J.*, **23**(3), 243-261. https://doi.org/10.12989/sss.2019.23.3.243

Pnevmatikos, N.G. and Gantes, C.J. (2011), "Influence of time delay and saturation capacity to the response of controlled structures under earthquake excitations excitations", *Smart Struct. Syst.*, *Int. J.*, **8**(5), 449-470. https://doi.org/10.12989/sss.2011.8.5.449

Saaed, T.E., Nikolakopoulos, G., Jonasson, J.E. and Hedlund, H. (2015), "A state-of-the-art review of structural control systems", *J. Vib. Control*, **21**(5), 919-937. https://doi.org/10.1177/1077546313478294

Tan, P., Dyke, S.J., Richardson, A. and Abdullah, M. (2005), "Integrated device placement and control design in civil structures using genetic algorithms", *J. Struct. Eng.*, **131**(10), 1489-1496. https://doi.org/10.1061/(ASCE)0733-9445(2005)131:10(1489)

Tejani, G.G., Pholdee, N., Bureerat, S., Prayogo, D. and Gandomi, A.H. (2019), "Structural optimization using multiobjective modified adaptive symbiotic organisms search", *Expert Syst. Applic.*, **125**, 425-441. https://doi.org/10.1016/j.eswa.2019.01.068

Wang, H., Liao, L., Wang, D., Wen, S. and Deng, M. (2014), "Improved artificial bee colony algorithm and its application in LQR controller optimization", *Mathe. Problems Eng.*, Article ID: 695637. https://doi.org/10.1155/2014/695637

Wongsathan, C. and Sirima, C. (2008), "Application of GA to design LQR controller for an inverted pendulum system", *Proceedings of 2008 IEEE International Conference on Robotics and Biomimetics*, February. Bangkok, Thailand.

Xiong, X. and Wan, Z. (2010), "The simulation of double inverted pendulum control based on particle swarm optimization LQR algorithm", *Proceedings of 2010 IEEE International Conference on Software Engineering and Service Sciences*, July, Beijing, China.

Xu, K. and Igusa, T. (1992), "Dynamic characteristics of multiple substructures with closely spaced frequencies", *Earthq. Eng. Struct. Dyn.*, **21**(12), 1059-1070. https://doi.org/10.1002/eqe.4290211203

Yang, D.H., Shin, J.H., Lee, H.W., Kim, S.K. and Kwak, M.K. (2017), "Active vibration control of structure by active mass damper and multi-modal negative acceleration feedback control

algorithm", *J. Sound Vib*., **392**, 18-30. https://doi.org/10.1016/j.jsv.2016.12.036

Zaeri, A.H., Poodeh, M.B. and Eshtehardiha, S. (2007), "Improvement of Cûk converter performance with optimum LQR controller based on genetic algorithm", *Proceedings of 2007 International Conference on Intelligent and Advanced Systems*, November, Kuala Lumpur, Malaysia.

BS